Lourenco Sorger, Goncalo; Sarikka, Teemu; Santos Vilaca da Silva, Pedro; Santos, Telmo G.

Effect of processing temperatures on the properties of high strength steel welded by FSW

Published in:
70th International Institute of Welding Annual Assembly and International Conference, IIW 2017

Published: 01/01/2017

Document Version
Peer-reviewed accepted author manuscript, also known as Final accepted manuscript or Post-print

Please cite the original version:
Lourenco Sorger, G., Sarikka, T., Santos Vilaca da Silva, P., & Santos, T. G. (2017). Effect of processing temperatures on the properties of high strength steel welded by FSW. In *70th International Institute of Welding Annual Assembly and International Conference, IIW 2017* Article III-1825-17

IIW Document No.: III-1825-17

Effect of processing temperatures on the properties of high strength steel welded by FSW

Gonçalo Sorger[1*], Teemu Sarikka[1], Pedro Vilaça[1], Telmo G. Santos[2]

[1] Department of Mechanical Engineering, School of Engineering, Aalto University, 02150 Espoo, Finland.
[2] UNIDEMI, Departamento de Engenharia Mecânica e Industrial, Faculdade de Ciências e Tecnologia, Universidade Nova de Lisboa, 2829-516 Caparica, Portugal.

[*] Contacting author: goncalo.sorger@aalto.fi

Abstract

The need for weight reduction without compromising load-bearing capacity has raised interest in the use of modern higher-strength steels (HSS). Recent advances in steelmaking have enabled the production of lean alloyed steels with exceptional mechanical properties allowing the design and fabrication of lighter, high-performance structures. Nevertheless, the ability to take full advantage of the improved properties of the modern HSS is dependent on their weldability. Conventional fusion welding methods are not suited for welding these materials since the high peak temperatures and cooling rates, during weld cycle, destroy their properties. Alternatively, the solid-state Friction Stir Welding (FSW) method can join the HSS at low peak temperatures, preserving some of the original properties of the base material. In this work, the influence on material properties of different peak temperatures and cooling rates during the FSW cycle was evaluated. A HSS produced by a thermo-mechanically controlled process, with a specified minimum yield stress of 700 MPa, was welded by FSW with peak temperatures, measured within the processed zone, ranging from about 900 ºC to 650 ºC. The plate thickness was 4 mm and square butt joints were welded with a single pass with different parameters, and cooling conditions. A water-cooled clamping and anvil system was custom designed and applied for this purpose. Temperatures were measured using thermocouples positioned in small holes drilled to the half-thickness of the workpiece, at distances of 5 to 10 mm from the joint line. The effect of the different peak temperatures was evaluated by mechanical testing, including bending, tensile testing with digital imaging correlation, Charpy impact test and hardness measurements. Microscopic analyses, including optical microscopy (OM) and electron backscatter diffraction (EBSD), were used to evaluate the microstructure. Results show that the FSW process enables the welding of HSS within the intercritical temperature domain, with the best weld condition having an impact toughness overmatching the toughness of the base material, from 138 % to 169 %, at both -40 ºC and -60 ºC. The yield strength efficiency was about 70 %.

Keywords: Friction stir welding; Temperature; High strength steels; Mechanical properties; Microstructure, Microscopy.

1. Introduction

Steels are the main engineering material used for construction and fabrication and welding is the most important and extensively used manufacturing technique applied to steels. Thus, the weldability of the steels is an essential property, and is currently a major limitation to the widespread use of the new special ultra-high strength steel (UHSS) [1]. The UHSS steels that have been manufactured using accelerated cooling to achieve the desired microstructures are generally not resistant to high heat inputs and the degradation of properties can occur when welded by conventional fusion processes. This is also because of the wide range of cooling rates within the weld region that encompasses cooling rates values from higher to lower than that of production. Compared to conventional fusion welding methods, friction stir welding (FSW) produces welds with significantly lower peak temperature, and typically lower heat input dissipated into the heat affected zone (HAZ) due to the high thermal efficiency, e.g. over 90 % when applied to aluminium alloys [2].

The distinction between high strength steel (HSS) and UHSS has not been universally defined by one precise strength level. A universal yield strength limit for UHSS would be difficult to define since the strength levels of special steels are continuously increasing as new steels are developed [3]. The steel studied in this paper has a yield strength of 700 MPa and is considered an UHSS based on the classification in reference [4], where the minimum yield strength for UHSS is 550 MPa. However, in some classifications considerably higher yield strengths are required. For example, in reference [5] yield strength of 900 MPa is required for the steel to be classified as an UHSS.

Thermo-mechanically controlled processing (TMCP) is nowadays a common production method for HSS and UHSS since it enables the production of steels with fine grain. High strength can thereby be achieved even with low levels of alloying. Furthermore, this is not accomplished at the expense of toughness as grain size is the key factor in achieving the high strength [1,6]. The lower amounts of alloying elements have the further advantage of reducing production costs [7,8]. These steels are quite sensitive to the peak temperatures and cooling rate to avoid destroying the original optimized grain size and good balance of strength and toughness properties. Friction Stir Welding (FSW) due to its solid-state process domain and autogenous nature can join these materials at significantly lower temperatures and with some control of the cooling rates via the clamping system, overcoming the weldability limitations of conventional fusion welding methods.

Friction Stir Welding is nowadays widely used across many market sectors in the fabrication of safety critical structures, mostly made for lightweight metals and their alloys [9]. FSW of aluminum [10,11], copper [12,13] and magnesium [14] has had excellent results once the operational parameters have been optimized. This success increased the interest in transferring the benefits of the process to other engineering materials such as modern steels. The lower processing temperatures associated with the FSW (compared to fusion welding processes) shows good potential to produce fewer metallurgical changes in the weld metal and HAZ and minimizes distortion and residual stresses in steels [15]. Furthermore, the absence of melting eliminates the susceptibility for hot cracking, and hydrogen induced cracking in steels. Also, it reduces hazardous fume emissions during welding [16].

The first publications on the FSW of steels are dated from 1997 using a FSW tungsten tool. During 1998, many trials were conducted leading to the production of FSW tools made of a W-25Re alloy which had shown improvement from the tungsten tools [17]. Still, it was only in 1999 that the feasibility of FSW of steel was firstly reported in open literature. Thomas et al. [18] showed that 12 mm plain low carbon steel and 12 % chromium alloy steel can be welded in a single pass, and demonstrated, by tensile and bend testing, that the mechanical properties of the welded joints of these materials can be compared to those of the base material. Tool wear was identified as a limitation but recent advances in material selection and design have led to the development of tools having a fine balance of high-

temperature strength, hardness and ductility enabling the production of long uninterrupted FSW steel welds [19,20].
Compared to fusion welding, FSW produces less distortion, is not detrimental to toughness and does not approach concerning levels of hardness. Additionally, FSW can produce superior fatigue properties [21]. The solid-state nature of the FSW process can enable joining the TMCP steels in the same range of temperatures where they are originally processed, i.e., the intercritical temperature region (ferrite austenite two phase region) between the A1 and A3 temperatures. FSW of UHSS in their optimal range of thermomechanical processing conditions can result in welds with fine microstructure where a good combination high strength and toughness is achieved. Furthermore, FSW is an autogenous process (i.e. it requires no filler metal), which helps to reduce or eliminate the chemical and mechanical mismatch in the processed zone.
Most of the studies on FSW of steels, such as the ones by Lienert et al. [22] and Reynolds et al. [23], reported that the stir zone of ferrous metals presents a recrystallized microstructure, like in the FSW of aluminum alloys. This indicates that FSW of ferrous metals develops in a similar way to that of aluminum. The trend is analogous to that observed with aluminum: as heat input is reduced, the grain size decreases and the strength gradually increases [24,25]. Additionally, complex phase transformations can occur in the FSW of steel. Accordingly, mechanical properties are improved compared to the base metals.
The microstructures and mechanical properties of FSW joints on carbon steel are significantly affected by the welding conditions. The strength of the steel joints increases with the decreasing heat input. This is attributed to the relationship between the peak temperature and the A1 to A3 domain temperatures. When FSW is performed within this intercritical temperature region the microstructure is refined and the highest strength is achieved [26]. Although in [26] FSW was applied to mild steels (IF steel, S12C and S35C) it is reasonable to assume that FSW of TMCP HSS with low heat-input, resulting in peak temperatures between A1 and A3, would have a similar, if not more relevant, effect. Since the improved properties of HSS and UHSSs typically result from thermomechanical processing within the A1 and A3 temperatures, FSW in this range of temperatures should prevent the loss of the original microstructure, including the typical refined grain. Additional evidence of the benefits, for UHSS, of FSW at temperatures in the intercritical temperature range was presented in [27]. Sound FSW welds performed on a 2.2 mm sheet metal 1600 MPa quenched and tempered UHSS with process temperatures above and below A1 were compared. The microstructure of the stirred zone processed above A1 is akin to that of the base material, with fine martensite and some retained austenite. Accordingly, the mechanical properties also comparable to those of the base material. In contrast, the microstructure of the stirred zone processed below A1 is markedly different, with fine ferrite and over tempered martensite. Thus, the main motivation for this research work is to evaluate the same potential benefits when applying the FSW to a thicker, 6 mm HSS plate with a specified minimum yield stress of 700 MPa.
In this work, the influence of different peak temperatures and heating and cooling rates achieved during the FSW cycles was evaluated. A TMCP HSS, with a specified minimum yield stress of 700 MPa, was welded by FSW under different conditions, resulting in peak temperatures in the processed zone ranging from about 650 ºC to 900 ºC. The effect of the different peak temperatures and heating and cooling rates on the microstructure and properties was investigated.

2. Experimental procedure

With the objective of preventing the processed zone from overcoming the intercritical temperature domain for low alloy steels, the experimental procedure consisted of FSW of a modern HSS plate with

four different conditions, combining a set of two parameters with an anvil system with and without cooling. The temperature was monitored in different key-positions of the processed zone and specimens were extracted for mechanical and microstructural characterization. The tests include bending, tensile, Charpy impact, hardness, optical microscopy (OM) and electron backscatter diffraction (EBSD).

Material

The material studied in this paper was the Strenx 700MC+ from SSAB, a modern hot-rolled structural HSS produced by TMCP. This direct quenched steel fulfils the requirements of the S700MC grade, according to standard EN 10149-2, with nominal chemical composition presented in Table 1. The plate thickness was 4 mm. Investigation on the weldability of this steel, in different thicknesses, by MIG, PAW and SAW was investigated by Peltonen [28] and Lathtinen [29].

Table 1 Chemical composition of the S700MC (wt. %), according to melting analysis conducted by SSAB in Raahe, Finland. The CE_{IIW} is the carbon equivalent according to according to International Institute of Welding based Dearden et al. [30].

	C	Si	Mn	Cr	Nb	Ti	V	Al
Material	0.056	0.179	1.8	0.048	0.082	0.112	0.012	0.036
S700MC	Cu	Ni	Mo	N	B	P	S	CE_{IIW}
	0.016	0.035	0.009	0.0068	0.0003	0.009	0.0022	0.241

FSW procedure specification

The weld runs were carried out in force control, using an ESAB Legio 5 UT FSW machine. The plate dimensions before welding were 330 mm(rolling and welding direction) x 100 mm. Four sets of welding conditions were produced, designated: 1) "Slow"; 2) "Fast"; 3) "Slow+Cooled", and 4) "Fast+Cooled" according to their different welding parameters (travel speeds) and external forced cooling condition. The sets of the most important constant and variable welding parameters and cooling conditions are presented in Table 2. The weld pitch ratio (Ω/v) used for the slow (hotter) welds was $(\Omega/v)_{slow} = 3.33$, and for the fast (colder) welds was $(\Omega/v)_{fast} = 1.67$. All welding runs were single-pass, square butt joint welds, in flat position. The edge preparation was done by machining. The plates were firmly clamped with mechanical fixtures and dedicated water cooled clamping elements and backing bar that enable active cooling as depicted in Figure 1a. The backing bar, or anvil, can also be water-cooled. The plates were joined using a tool made from pcBN-based W-Re composite materials with 70 vol. % pcBN [31]. The tool has a scrolled convex shoulder with outer diameter of 25 mm and a 3.75 mm long conical probe with stepped spiral features. Other relevant features of the tool are identified in Figure 1b. As shielding gas for the tool and processed zone, Argon was used with a flow of 20 l/min out of a nozzle with diameter of 70 mm, involving the body of the FSW tool. The parameters used during the plunging period, were a rotation speed Ω = 800 rpm, plunging speed of v_z = 0.1mm/s, plunging depth z_{plunge} = 3.9 mm and t_{dwell} = 3 s. The weld length was 290 mm starting and ending 20 mm from the edge of the plates.

Table 2 FSW set of parameters for the different weld conditions.

FSW Condition	F [kN]	Tilt angle [º]	Ω [rpm]	v [mm/min]	Cooling
Slow	45	0	200	60	Off
Fast				120	Off
Slow + Cooled				60	On
Fast + Cooled				120	On

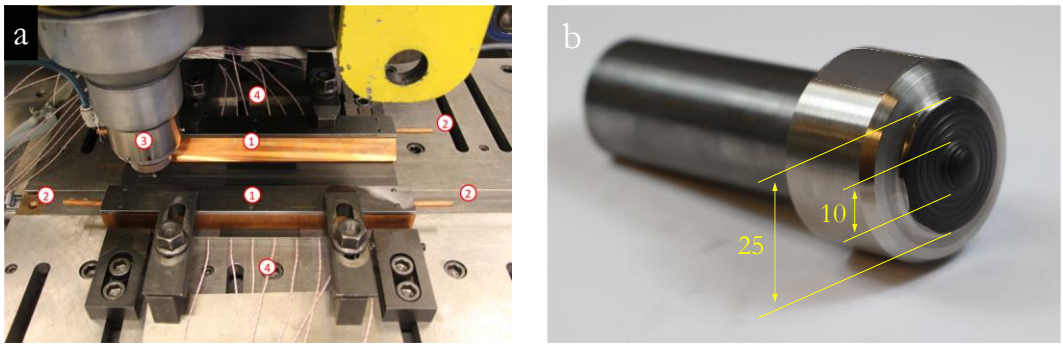

Figure 1 - Welding setup and tool for FSW: a) Details on the clamping system and temperature measurement setup including: 1 - water cooled clamping elements; 2 - water cooled anvil; 3 - shielding gas nozzle; and 4 - thermocouple cables; b) FSW tool with shoulder and probe base dimensions.

Temperature measurements

For each of the four welding conditions, three plates were welded with same processing conditions. Among the three welded plates, one was used for in-depth temperature monitoring and to extract samples for bending tests. The remaining two welded plates were used for extraction of samples for tensile, Charpy impact and microscopy testing. The temperatures were measured at the half-thickness of the plates and at four different distances from the original abutting surfaces using insulated N-type thermocouples. The temperature measurement positions were ±10, ±8, ±6 and ±5 mm, where the positive (+) values represent temperatures measured at the advancing side (AS) and the negative (-) values represent temperatures measured on the retreating side (RS). These positions were chosen considering the tool geometry, to attempt to encompass all the different welding zones, while minimizing any disturbance to the material flow during the FSW process, e.g. avoiding direct contact with the probe (Figure 2a). Each measurement position was repeated once, for redundancy. Accurate positioning of the thermocouples was possible by employing a backing plate with grooves machined for the thermocouple wires and by drilling holes in the weld plates at the desired temperature measurement positions and depth as depicted in Figure 2b. The distance between the measuring cross-sections positions along the weld direction was 25 mm, over one shoulder diameter to ensure no coercive effect in the thermal field, between the different cross-sections where the thermocouples are inserted.

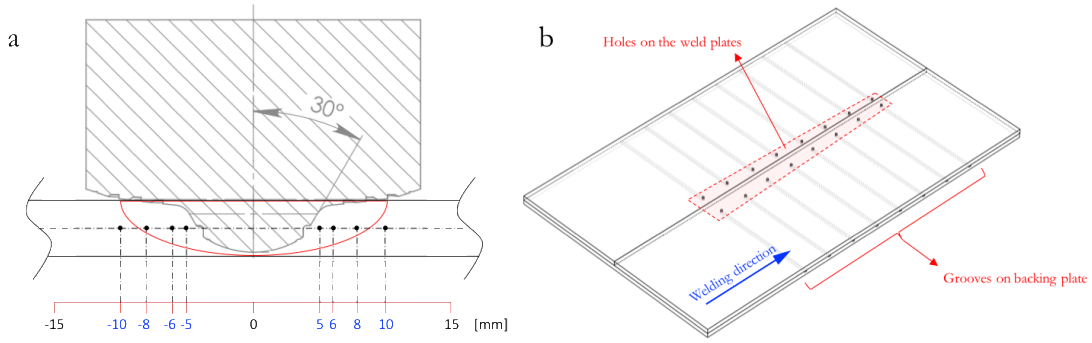

Figure 2 - Schematic representation of the thermocouple positions: a) the thermocouple positioning at each of the cross-sections; and b) the temperature measurement positions along the weld joint in relation to the weld direction.

Mechanical and microscopy testing

Bending testing - Specimens for bending tests were extracted from the first weld of each set, at positions that were unaffected by the thermocouple positioning holes. For each of the four welding conditions, six bending specimens were tested, three with the tension stress at the face side, and three with tension at the root side. The bending tests were carried out according to standard ISO 5173 + A1, using a MTS 810 Material Test System at a constant speed of 0.2 mm/s. The maximum displacement of the loading pin was restricted to 60 mm from the starting position contacting the surface of the specimens.

Tensile testing and DIC measurements - Specimens for tensile testing were extracted from the second and third welds of each welding condition according to the extraction plan presented in Figure 3a. The tensile tests were conducted using a MTS Landmark machine. A 25 mm extensometer was used to register the strain rate. For one specimen of each condition digital image correlation (DIC) measurements were performed. A Lavision Imager Pro X camera system was used and pictures of the specimens were taken at the frequency of 2 Hz during the tensile test. A random pattern was spray painted on the specimens over a white paint substrate. Based on changes in the pattern with increasing strain, the behavior of the strain and its localization was estimated by analyzing the images using DaVis software.

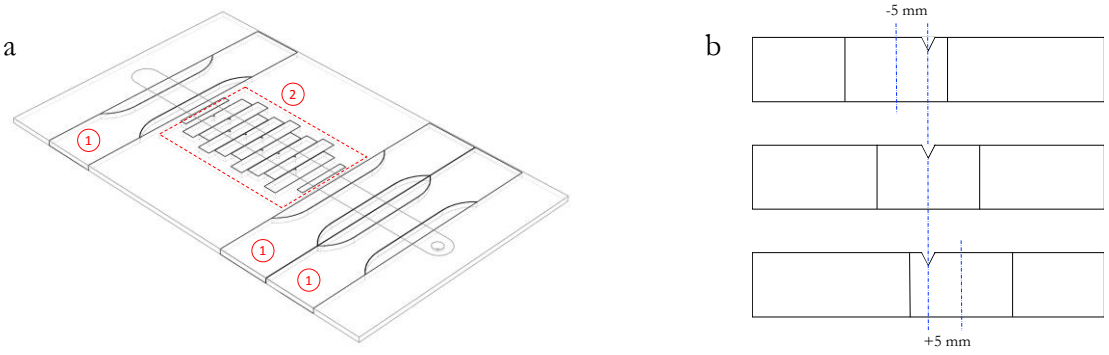

Figure 3 - Specimen extraction plan for tensile specimens (1), and Charpy impact specimens (2): a) Specimen extraction plan; and b) Detail of the Charpy notch positions relative to the weld center (stirred zone), weld center +5 mm (advancing side), and weld center -5 mm (retreating side).

Charpy impact testing - The Charpy impact tests were conducted according to standard ISO 148-1. Due to constraints posed by plate thickness, a reduced-section, i.e. sub-size specimen, was used [mm]: 55 x 10 x 4. The notches were placed at three different positions as illustrated in Figure 3b, corresponding to the center of the stirred zone (SZ), center -5 mm at the RS, and center +5 mm at the AS. The specimens were tested at -40 °C and -60 °C. Due to the non-standard size of the specimens, and to allow for a meaningful comparison and interpretation of the results, specimens with similar size were also extracted from base material and tested.

Hardness - The microhardness measurements were performed using an instrumented tester and a Vickers tip with a step size of 0.5 mm and an indentation load of 5 N (roughly equivalent to HV05) producing indentations with a cross-section diagonal of approximately 50 μm in the base metal. The measurements matrices, containing 315 indentations, matrices covered a 22.5 mm by 3.5 mm area encompassing the different weld zones and the BM on both sides of the weld.

OM and EBSD - Specimens for optical microscopy were polished down to 1 μm diamond paste and etched with 2 % nital solution. The optical micrographs were taken using an Olympus CX40 microscope. The microscope was equipped with Olympus MPlan metallurgical lenses. SEM/EBSD studies were carried out using a Zeiss Ultra 55 field emission scanning electron microscope (FESEM) equipped with an HKL Nordlys EBSD detector by Oxford Instruments. Sample preparation for EBSD was conducted using a mechanical vibratory fine polishing to ensure a deformation-free surface to obtain a sufficiently high diffraction pattern quality. The EBSD data was post-processed using Channel 5 post-processing software.

3. Analysis of results

Temperature measurements

The highest temperatures for all the weld conditions were measured by the thermocouples positioned closest to the FSW tool, i.e. at ±5 mm distance. The difference between the temperatures measured at the RS and AS are small, i.e. less than 25 ºC, with slightly higher values at the RS. Thus, for convenience of the comparison between the different weld conditions, only the temperatures acquired at the RS are presented. Table 3 presents the highest temperatures recorded on each weld. The highest peak temperature was reached during the Slow weld, 906.2 ºC, while the Fast+Cooled weld achieved the lowest peak temperature, 656.3 ºC. The Fast and the Slow+Cooled welds reached intermediate peak temperatures of 761.1 ºC and 741.1 ºC, respectively. The active cooling of the clamping system presents a more relevant role than the welding speed in controlling the peak temperature. Besides its effect on the peak temperatures, the influence of the active cooling can also be seen to be more relevant than the weld pitch ratio (Ω/v) during the thermal history, mainly during the heating period, but also during the cooling period, as presented in Figure 4a. Figure 4a shows that the temperature increase is much faster in the +Cooled welds than in the non-cooled ones. Comparing the heating phase of the Fast and the Slow+Cooled welds, which reach similar peak temperatures, further emphasizes this effect. Naturally, the cooling times are also smaller for the +Cooled welds. Since only the Slow weld reached a peak temperature above 800 ºC it is not possible to compare the $t_{8/5}$ cooling times for the four welds. Alternatively, the cooling times from 600 ºC to 500 ºC ($t_{6/5}$) are presented in Figure 4b.

Table 3 Peak temperatures recorded at the four different weld conditions.

Weld	Slow	Fast	Slow+Cooled	Fast+Cooled
T_{max} [ºC]	906.2	761.1	741.1	656.3

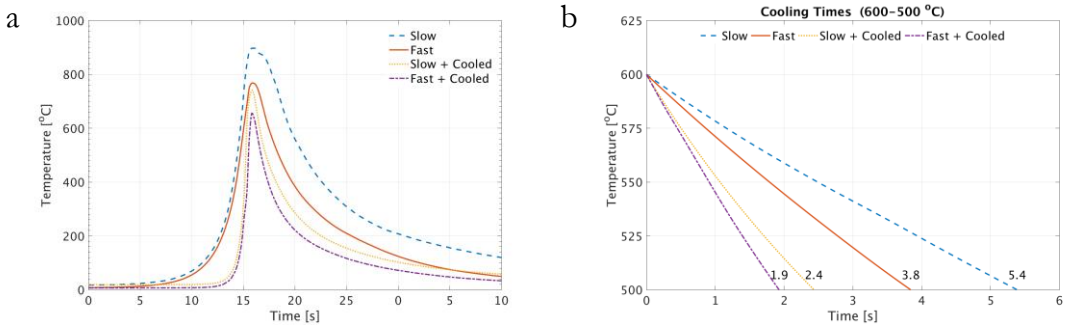

Figure 4 – Results from the temperature monitoring for the different weld conditions at -5 mm distance from the joint line, i.e. at the retreating side (RS): a) Temperature history; b) Detail of the cooling times from 600 ºC to 500 ºC ($t_{6/5}$).

Between the weld conditions with higher weld pitch ratio, i.e. the slow welds, the cooling rate without active cooling is 18.5 ºC/s, and with active cooling it is 41.7 ºC/s (an increase of 225 %). For the weld conditions with lower weld pitch ratio, i.e. the fast welds, the cooling rate without active cooling is 26.3 ºC/s, and with active cooling is 52.6 ºC/s (an increase of 200 %).

Microstructure analysis

The macrographs of the four different weld conditions are presented in Figure 5. The most significant difference between the weld beads is the fact that the width of the processed zones are narrower in the +Cooled welds, mainly at the top surface, and their heat affected zones (HAZ) are much smaller. Thus, these results are in line with the thermal analysis results presented previously. With the active cooling, not only the peak temperatures are lower, but also the time above critical temperatures is significantly reduced. From the macrographs, it is possible to conclude that the active cooling has a very relevant effect in the overall geometry of the weld beads, when compared with changes in travel speed. Figure 5d, corresponding to the Fast+Cooled weld, depicts a void defect present at the AS of the lower section of the stirred zone. This fact indicates that the cold conditions were taken to an extreme for the FSW of steels, where the level of viscosity within the stirred material wasn't low enough for a correct material flow and complete consolidation of the stirred zone.

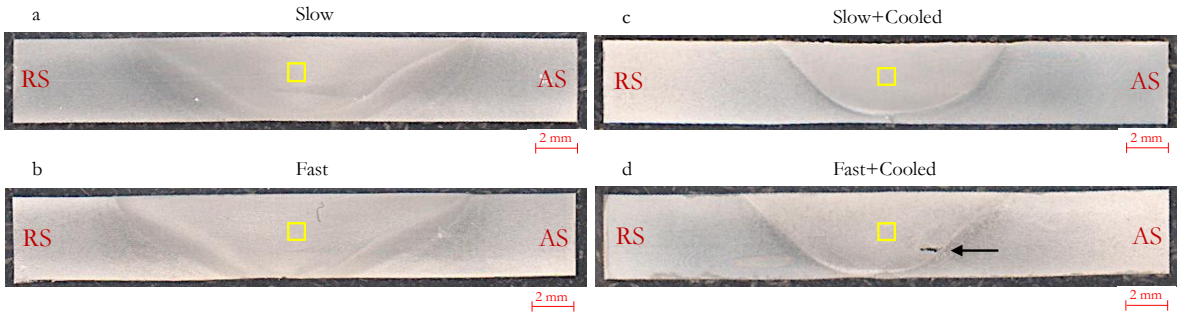

Figure 5 - Macrographs of the cross-section of each of the four different weld conditions (yellow square marks position of micrographs and EBSD): a) Slow weld; b) Fast weld ; c) Slow+Cooled weld; d) Fast+Cooled weld, where the arrow points to a void defect.

Another evidence of the effect of the temperature within the stirred zone, is the level of penetration of the stirred zone and processing of the root of the welds. In the Slow and Fast welds, Figure 6a and

Figure 6b, respectively, there is full penetration with evidence of some small and discontinuous alignment of oxide particles. On the other hand, Figure 7c and Figure 6d, reveal that the +cooled welds resulted in defects of lack of penetration (LOP) welds. Therefore, for half of the specimens for tensile test, and one specimen for the bending test, with the root on tensile, 0.5 mm of the root side were removed by milling. The mechanical results will present data for machined and non-machined conditions, for the same weld condition. This strategy was implemented to decouple the effect of the incomplete penetration, from the microstructural changes induced by the thermomechanical processing during the FSW cycle.

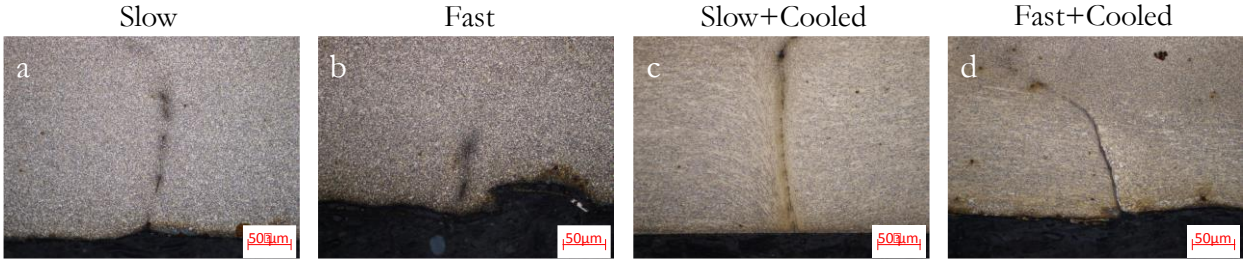

Figure 6 - Micrographs of the welded samples showing a detail of the weld roots at 20x magnification. The non-cooled welds (a,b) present almost full penetration with some oxide alignment. The +Cooled welds (c,d) exhibit some lack of penetration due to localized cooling effect from the cooled anvil.

The microstructure of the HSS base material (BM), the micro alloyed S700MC grade, consists of fine grained ferritic-bainitic microstructure produced by rolling and direct quenching. The elongated grains along the rolling direction, presented in Figure 7a, show a strong effect of the original TMCP production cycle in the microstructure of the BM. The grain size of the BM is 1.73 μm (Table 4). The Figure 7b-e, show a significant contrast of the microstructure in the stirred zone of the welds when compared with the one from the BM. The FSW produced a dynamically recrystallized zone, retaining some ferritic-bainitic microstructure, but with increased presence of ferrite. The grains are fine equiaxed, with sizes of about 1.8 μm, for the welds without active cooling, and of about 1.3 μm with active cooling, as depicted in Table 4. Again, in the grain size, the active cooling played a more relevant role compared with the weld pitch ratio (Ω/v).

The Figure 8, presents the EBSD images for the original HSS and for the stirred zones of the different welding conditions. The band contrast images highlight the grain geometry and size already presented in the Figure 7 and Table 4. The inverse pole figures show a contrast between the orientation of the microstructure of the BM where a texture effect exists with dominating <101> direction, and that of the stirred zones with more randomly oriented grains. The local misorientation maps show the local concentration of higher strain (green colour) in the base material than in the stirred zone of the welds. This fact will support the hardness maps of the cross section of the welds.

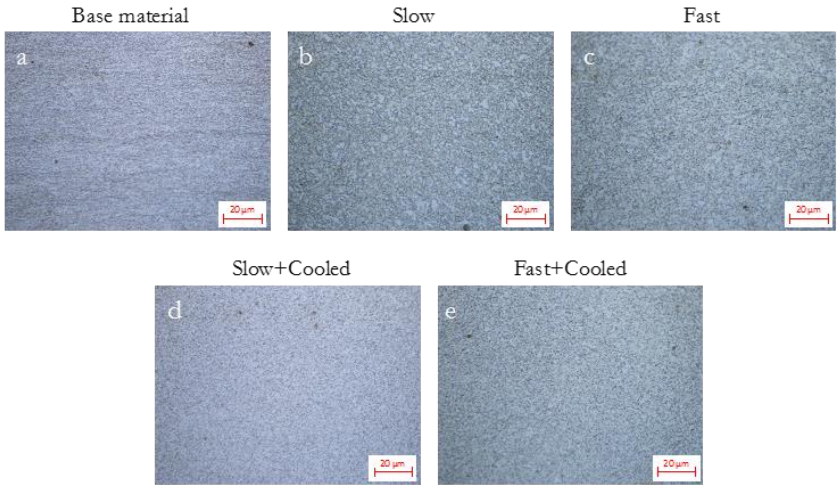

Figure 7 - Micrographs (OM with 50x magnification) of the base material and middle of the stirred zone of the four different weld conditions: a) Base material b) Slow weld; c) Fast weld ; d) Slow+Cooled weld; e) Fast+Cooled weld.

Table 4 Average grain size in the base material and in the stirred zone of the four different weld conditions.

Grain size	Base Material	Slow	Fast	Slow+Cooled	Fast+Cooled
ISO [μm]	1.73	1.81	1.81	1.26	1.38
ASTM [μm]	2.56	2.70	2.65	1.89	2.00

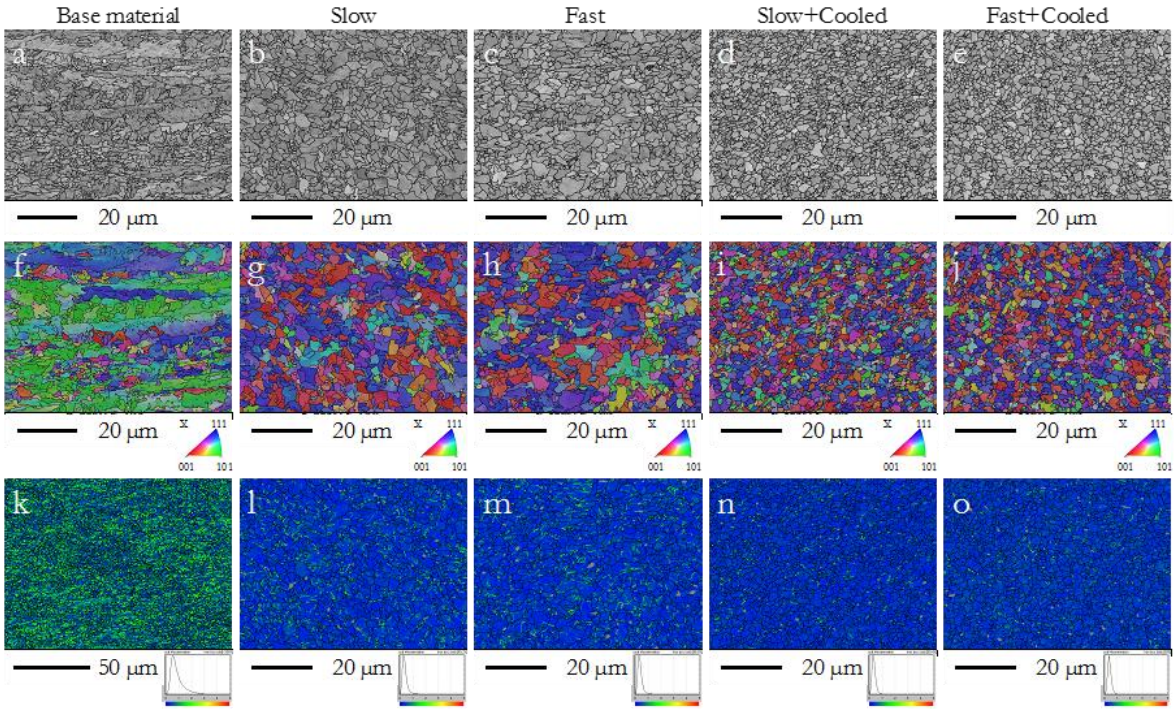

Figure 8 - EBSD images for the base material and for the stirred zones of the different weld conditions: a-e) The band contrast images; f-j) The inverse pole figures showing the orientation of the microstructure; k-o) The local misorientation maps.

Hardness test results

The hardness maps obtained from the different weld conditions are presented in Figure 9. The base material hardness is about 275 HV05. The pattern is similar in all the welds, with a significant drop of the hardness in the stirred zone (average of 220 HV05), increasing sharply from the boundary of the thermomechanically affected zone (TMAZ) into the HAZ where it reaches around 320 HV05. There is a somewhat higher hardness zone (270 HV05), at the AS near the root in the stirred zone of the Slow and the Fast welds (i.e. those without active cooling). This effect is most probably due to a local concentration of precipitates led by the material flow during the FSW process. This concentration of precipitates can be seen in the macrographs of Figure 5a and Figure 5b. In the welds without active cooling, the RS presents the higher values, with a maximum of 407 HV05 at the Slow weld, maybe due to a fast cooling from relative higher peak temperatures. The distribution of the hardness at the HAZ around the stirred zone is more uniform, for the welds with active cooling.

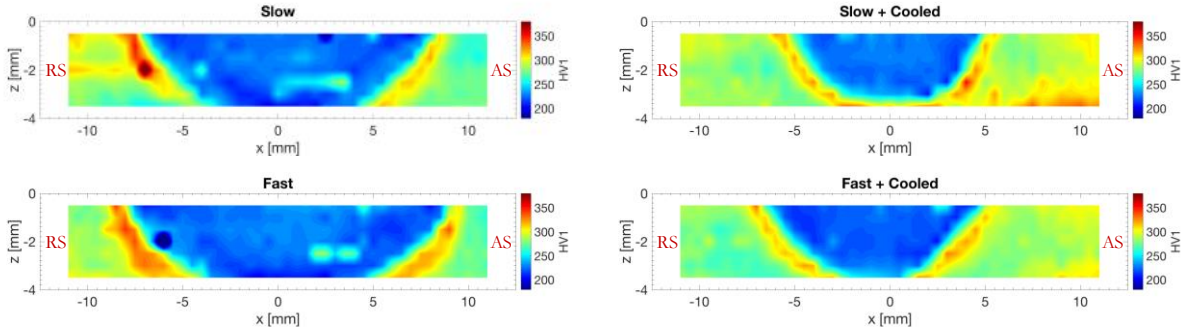

Figure 9 - Hardness (HV05) distribution maps of the four different weld conditions.

Bending and tensile test results

The results of the bending tests (Figure 10) with the face side in tensile, present an efficiency between 90 % and 94 % for all the weld conditions. The root defect plays an important role in all the tests with the root in tensile (efficiency less than 60 %), with exception of the Slow weld condition that presents a high efficiency. The machined specimens with the root in tensile, have an efficiency between 79 % and 84 %, slightly lower than with the face in tensile. In general, the weld conditions only affects the resistance under bending load if the root defect reaches a relevant size, e.g. over 50 μm of continuous alignment of particles or LOP.

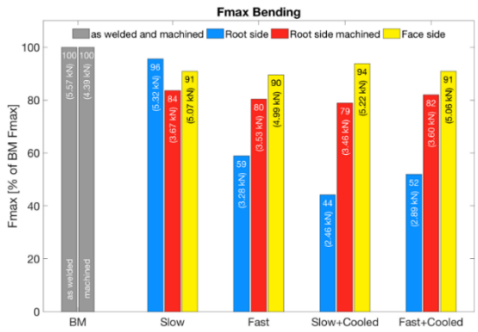

Figure 10 - Maximum bending force with results for all the four weld conditions presented in absolute values and in percentage relative to the base material (BM).

The results of the tensile strength of the welds are presented in Figure 11 and show to be dominated by the lower strength at the stirred zone. There is a reduction in yield strength from the original 787 MPa to 537-571 MPa, which means an efficiency of about 70 %. The reduction in ultimate tensile strength (UTS) is about 21 %.The localization of the strain is always at the middle of the weld, within the stirred zone as exhibited in Figure 12. This localization effect is more distributed when there is no relevant root defect, as in the Slow weld condition. In fact, only the Slow weld condition presents same deformation pattern at the UTS and before fracture, between the as-welded and machined specimens. In general, neither the weld condition, nor the small root defect shown to affect the strength of the weld under tensile loading condition.

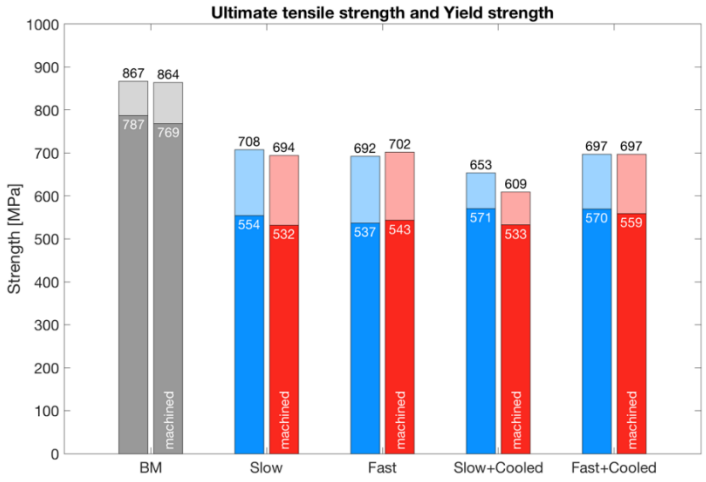

Figure 11 - Tensile test results showing the ultimate tensile strength (UTS) and yield strength of the base material (BM) and the four different weld conditions.

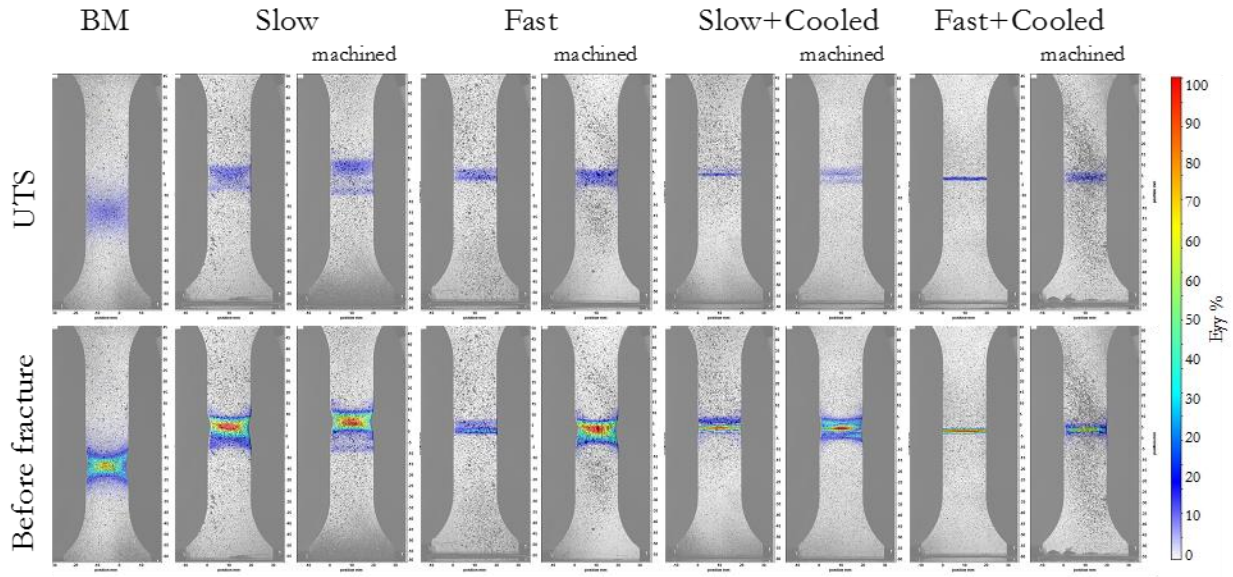

Figure 12 – Digital image correlation (DIC) images monitoring the strain field during the tensile tests, for the base material (BM) and the four different weld conditions, with specimens in as-welded and machined condition. The strain field is presented at the moment when the UTS is reached (top) and immediatly before fracture (bottom).

Charpy impact tests results

The impact toughness of the welded zone is one major challenge on the weldability analysis of HSS [29]. The results of the Charpy impact tests of the FSW of this S700MC grade steel, are presented in Figure 13, measured at the three locations identified in Figure 3, at -40 ºC and -60 ºC. From a global analysis of the results, all the weld zones of all the weld conditions closely matches or in most of the situations, overmatches the base material properties: 41 J@-40 ºC, and 39 J@-60 ºC. The trend in all the weld conditions repeats at both temperatures. Namely, the stirred zone is the best zone of the weld in the Fast+Cooled and the worst in the Slow welds. The Fast weld condition presents the best global results, with quite homogeneous values in all the weld region and overmatching the toughness of the base material at both temperatures, from 138 % to 169 %. The Slow+Cooled weld is the worst weld condition at both temperatures. The RS is distinguishably better than the AS for the welds Slow and Fast (i.e. with no active cooling), and more homogeneous for the welds with active cooling, in line with the hardness maps presented in Figure 9.

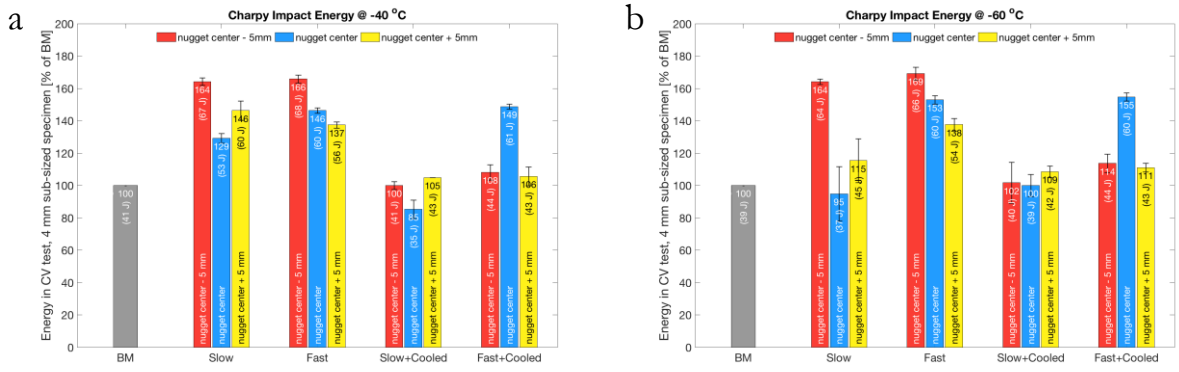

Figure 13 - Charpy impact results at the nugget center -5 mm (i.e. retreating side), nugget center and nugget center +5 mm (i.e. advancing side). The results are presented in absolute values and in percentage relative to the base material (BM): a) Test at -40 ºC; b) Test at -60 ºC.

4. Conclusions

Extensive microstructure and mechanical testing evaluated the effect of the different weld conditions, targeting cold weld conditions with different peak temperatures and cooling rates. The main results are as follows:

- The FSW process enables the welding of HSS within the intercritical temperature domain. The highest peak temperature at 5 mm from the joint line was 906.2 ºC reached during the Slow welds, while the Fast+Cooled welds achieved the lowest peak temperature of 656.3 ºC;
- The active cooling of the clamping system presents a more relevant role than the weld pitch ratio (Ω/v) in controlling the peak temperature, heating and cooling rates. The influence of the active cooling in cooling rates is over 200 % over the Slow and Fast weld conditions;
- The active cooling has a very relevant effect in the overall geometry of the weld beads, when compared with changes in the weld pitch ratio (Ω/v). The width of the processed zones are narrower in the active cooled welds, mainly at the top surface, and their HAZs are smaller;
- Extreme FSW cold conditions may lead to defects in the stirred zone, such as voids and root defects;

- The FSW produced a stirred zone with fine equiaxed grains, eliminating the original orientation although retaining some of the ferritic-bainitic microstructure.
- The grain size in the stirred zone was 1.8 μm, for the welds without active cooling, and 1.3 μm with active cooling, which means that the original small grain size of about 1.73 μm, resulting from the TMCP manufacturing process of the BM, was also retained;
- The local misorientation maps from the EBSD analysis show higher strain concentration of strain in the base material than in the stirred zone of the welds. This fact supports the reduction of the hardness in this region of all the weld conditions;
- The hardness drops from the 275 HV05 at the BM into 220 HV05 in the stirred zone, and increases sharply from the boundary of the TMAZ into the HAZ where it reaches around 320 HV05;
- The distribution of the hardness at the HAZ around the stirred zone is more uniform for the welds with active cooling;
- The bending tests present an efficiency of over 79 %, in relation to the BM, and the results show no sensitivity to the weld conditions except if the root defect reaches a relevant size;
- In all the weld sub-zones, and for all the weld conditions tested, the impact toughness of the FSW of these HSS, matches, or overmatches (in most of the situations) the base material properties at -40 ºC and -60 ºC;
- The Fast weld condition presents the best global impact toughness results, with quite homogeneous values across all the weld region, overmatching the toughness of the base material, at both temperatures, from 138 % to 169 %;
- The yield strength efficiency was about 70 %. The reduction in ultimate tensile strength (UTS) is about 21 %;
- In general, neither the weld condition, nor the small root defect affected the strength of the weld under tensile loading condition.

5. References

[1] Bhadeshia H and Honeycombe R (2011) Steels: microstructure and properties. Butterworth-Heinemann.

[2] P. Vilaça, L. Quintino, J. F. dos Santos (2005) iSTIR – Analytical thermal model for friction stir welding. Materials Processing Technology, 169(3):452-465.

[3] Philip T and McCaffrey T (1990) Ultrahigh-Strength Steels. in ASM Handbook - Properties and Selection: Irons, Steels, and High-Performance Alloys, Vol 1. ASM International, pp 430–448.

[4] Keeler, Kimchi M, Mooney P (2017) Advanced High-Strength Steels Application Guidelines Version 5.0, WorldAutoSteel, World steel association.

[5] Hall A M (1971) Introduction to today's ultrahigh-strength structural steels. American Society for Testing and Materials, Philadelphia.

[6] Tamura I, Ouchi C, Tanaka T, Sekine H, (1988) Thermomechanical processing of high strength low alloy steels, Butterworth & Co.

[7] Dhua S, Sen S (2011) Effect of direct quenching on the microstructure and mechanical properties of the lean-chemistry HSLA-100 steel plates. Mat Sci Eng A-Struct 528:6356–6365.

[8] Fukumoto Y (1996) New constructional steels and structural stability. Eng Struct 18:786-791.

[9] Vilaça P, Thomas W (2012) State-of-the-art in FSW technology In: Moreira PMGP et al (ed) Structural Connections for lightweight metallic structures. Springer, pp 85–124.

[10] Vidal C, Infante V, Vilaça P (2009) Fatigue behaviour in friction stir welded joints of AA2024 treated by improvement techniques. Weld World 53:241-246.
[11] Taavitsainen T, Vilaça P, Mutanen T (2016) Production by FSW of free-shape hollow box profile in AA5754 for automotive application. Weld World 60:1121–1131.
[12] Leal R M, Leitão C, Loureiro A, Rodrigues D M, Vilaça P (2010) Microstructure and Hardness of Friction Stir Welds in Pure Copper. Mater Sci Forum 86:637-642.
[13] Savolainen K, Saukkonen T, Mononen J, Hänninen H (2008) Entrapped Oxide Particles in FSWelds of Copper. 7th International Symposium on FSW. Awaji Island, Japan.
[14] Kannan B M, Dietzel W, Zeng R, Zettler R, dos Santos J F (2007) A study on the SCC susceptibility of friction stir welded AZ31 Mg sheet. Mater Sci Eng A-Struct, 460-461:243-250.
[15] McPherson N A, Galloway A M, Cater S R, Hambling S J (2013) Friction stir welding of thin DH36 steel plate. Sci Technol Weld Joi 18:441-450.
[16] Gomes J F P, Albuquerque P C S, Miranda R M, Vieira M T F (2012) Determination of Airborne Nanoparticles from Welding Operations, J Toxicol Env Heal A, 75: 747-755.
[17] Johnson R, (2005) Friction Stir Welding Steels - Status Report". TWI Members Report 838/2005.
[18] Thomas W M, Threadgill P L, Nicholas E D (1999) Feasibility of friction stir welding steel. Sci Technol Weld Joi 4:365-372.
[19] Rai R, De A, Bhadeshia H, DebRoy T (2011) Review: friction stir welding tools. Sci Technol Weld Joi, 16:325.
[20] Perrett J, Martin J, Peterson J, Steel R, Packer S (2011) Friction Stir Welding of Industrial Steels, presented at TMS Annual Meeting, San Diego, CA, USA.
[21] Azevedo J, Infante V, Quintino L, dos Santos J (2014) Fatigue Behaviour of Friction Stir welded steel joints. Advanced Materials Research, 891-892:1488-1493.
[22] Lienert T J, Stellwag W L, Grimmett B B, Warke R W (2003) Friction Stir Welding Studies on Mild Steel. Weld J, 82:1s-9s.
[23] Reynolds A P, Tang W, Posada M, DeLoach J (2003) Friction stir welding of DH-36 steel. Sci Technol Weld Joi, 8:455-460.
[24] Fujii H (2011) Friction stir welding of steels. Welding International, 25:260-273.
[25] Wei L, Nelson T W (2012) Influence of heat input on post weld microstructure and mechanical properties of friction stir welded HSLA-65 steel. Mater Sci Eng A-Struct, 556:51–59.
[26] Fujii H, Cui L, Tsuji N, Maeda M, Nakata K, Nogi K (2006) Friction stir welding of carbon steels. Mater Sci Eng A-Struct, 429:50–57.
[27] El-Batahgy AM, Miura T, Ueji R, Fujii H (2016) Investigation into feasibility of FSW process for welding 1600 MPa quenched and tempered steel. Mater Sci Eng A-Struct, 651:904–913.
[28] M. Peltonen (2014) Weldability of high strength steels using conventional welding methods. MSc thesis in Technology. Aalto University, Finland.
[29] T. Lahtinen (2016) Analysis and development of weldability of novel 700 MPa high strength steels. MSc thesis in Materials Science. Tampere University of Technology, Finland.
[30] J. O'Neill and H. Dearden (1940) A guide to the selection and welding of low alloy structural steels. Transactions of the Institute of Welding, 3:203–214.
[31] J Perrett, J Martin, J Peterson, R Steel and S Packer (2011) Friction stir welding of industrial steels, Friction Stir Welding and Processing VI, 65-72.